Febrile temperature enhances *Plasmodium falciparum* cytoadhesion by disrupting the endothelial glycocalyx

Viola Introini[1,2,3*#], Rory KM Long[1#], Olawunmi R Oyerinde[1], María Gestal-Mato[2,3], Leticia Hartmann[1,4], Silvia Sanz Sender[1], Frank Stein[5], Gyu Min Hwang[1,6], Borja Lopez Gutierrez[1], Karl B Seydel[7,8,], Gretchen Birbeck[8,9,10], Maria Bernabeu[1*]

[1] European Molecular Biology Laboratory (EMBL) Barcelona, Barcelona, Spain
[2] Max Planck Institute for the Science of Light, Erlangen, Germany
[3] Max-Planck-Zentrum für Physik und Medizin, Erlangen, Germany
[4] Faculty of Health and Medical Sciences, University of Copenhagen
[5] European Molecular Biology Laboratory (EMBL) Heidelberg, Proteomics Core Facility, Heidelberg, Germany.
[6] Heidelberg University, Faculty of Engineering Sciences, Heidelberg, Germany
[7] Department of Osteopathic Medical Specialties, College of Osteopathic Medicine, Michigan State University, East Lansing
[8] Blantyre Malaria Project, Kamuzu University of Health Sciences, Blantyre, Malawi
[9] Epilepsy Division, Department of Neurology, University of Rochester, Rochester, New York
[10] University Teaching Hospitals Neurology Research Office, Lusaka, Zambia

[#] Equal contribution

*Correspondence
maria.bernabeu@embl.es
viola.introini@embl.es

Abstract

Fever, a universal host defense in infection and inflammation, paradoxically contributes to neurological complications in malaria. While febrile temperatures enhance the expression of parasite virulence proteins that mediate vascular adhesion and disease severity, its effects in the endothelium remain elusive. Here we present a 3D fever-on-a-chip model that recapitulates human brain and lung microvessels under febrile conditions. Short febrile episodes at 40 °C, common in treated cerebral malaria patients, rapidly enhanced iRBC and immune cell binding under flow. Mechanistically, we demonstrated that this phenotype was driven by endothelial glycocalyx shedding, which exposed endothelial receptors EPCR and ICAM-1. Preserving glycocalyx integrity with a broad MMP inhibitor prevented the temperature-induced rise in cytoadhesion. These findings identify fever as a host-specific amplifier of vascular pathology in malaria and highlight endothelial-protective or antipyretic interventions as important strategies to mitigate febrile microvascular pathology.

Main

Fever is an ancient and metabolically costly host response to infection and inflammation, conserved across vertebrates. This tighly regulated process is initated when injury- and pathogen-associated molecular patterns trigger immune response and cellular secretion of prostaglandin E2 (PGE2)[1,2], a lipid effector molecule that activates thermoregulatory neuronal circuits in the hypothalamus to rapidly elevate core body temperature[3]. By transiently raising body temperature, fever restricts microbial fitness, slowing replication, and promoting immune clearance of diverse viral and bacterial pathogens[4]. Yet, fever prevention improves outcomes in diseases such as sepsis[5], neurological injury[6], and malaria[7], highlighting that it is not universally beneficial for the host.

Fever is a hallmark of malaria infection and a consistent predictor of severity[8,9]. A detrimental role of fever has been recently exemplified by seizure reduction after aggressive antipyretic treatment[10]. Central to severe malaria pathogenesis is the cytoadherence of *P. falciparum*-infected red blood cells (iRBCs) to the vascular endothelium[11], mediated by clonally variant *P. falciparum* erythrocyte membrane protein 1 (PfEMP1) proteins[12,13] with binding to intercellular adhesion molecule 1 (ICAM-1) and endothelial protein C receptor (EPCR) strongly linked with severe disease[14]. On the parasite side, febrile temperatures profoundly reshape iRBC biology[15] inducing cytoskeletal remodelling[16] and accelerating PfEMP1 surface expression[,17–19], changes that mechanically translate into rapid increase in iRBC stiffness[20], adhesion[21,22], and endothelial contact[19]. At the immune level, fever mobilises host systemic innate and adaptive immune responses,

63 promoting neutrophil and T cell vascular recruitment[23] and cytokine release[24]. Altogether, these findings
64 position fever as a potent promoter of vascular interaction with both iRBCs and immune cells. Yet studies
65 have focused almost exclusively on pathogen-driven mechanisms, leaving the endothelial response to
66 febrile temperatures poorly understood — a critical gap for host-directed therapeutic strategies.
67 Here, we employ a bioengineered human fever-on-a-chip microvascular model to dissect how febrile
68 temperatures affect the endothelium and regulate *P. falciparum* iRBC and immune cell adhesion.

69 **Paediatric patients experience high fever despite antipyretic treatment**

70 To characterise febrile dynamics in malaria, we analysed continuous temperature recordings from 146
71 children enrolled in a randomised controlled trial of aggressive antipyretic treatment for malaria Zambia
72 and Malawi. All participants presented central nervous system symptoms including impaired consciousness
73 and/or seizures, and 72–83% fulfilled the clinical definition of cerebral malaria (CM)[7,10]. Core temperature
74 was measured every 2-4 minutes over 72 hours using a monitoring patch. The present analysis was restricted
75 to children in the control group, who received World Health Organisation (WHO)-recommended treatment
76 with acetaminophen for temperatures over 38.5°C. Despite antipyretic therapy, all patients developed fever,
77 with 25% reaching body temperatures between 39-40 °C, and 10% reaching ≥ 40 °C (**Fig. 1a**). The average
78 fever duration was 1 hour for ≥ 40 °C and 1.7 hours for ≥ 39 °C, with some episodes persisting for several
79 hours (**Fig. 1b**). These findings demonstrate that short episodes of fever are common in CM patients, even
80 under current WHO-recommended fever management.

81 **Febrile temperature increases iRBC binding in 3D brain microvessels**

82 To determine whether hyperthermia influences *P. falciparum* binding to endothelial cells, we employed a
83 bioengineered 3D microvascular model that replicates flow-driven cytoadherence. The platform consists of
84 a microfluidic network of 13x13 channels of 120 µm diameter embedded in a collagen hydrogel,
85 recapitulating a wide range of flow velocities spanning 0.4–15 mm s^{-1} – comparable to those found in the
86 brain arteriovenous microcirculation (0.4–8 mm s^{-1})[25,26] (**Fig. 1c**). The device displays regions exposed to
87 a wall shear stress (WSS) > 1 dyn/cm^2 being representative of physiological flow observed in healthy
88 venules (1–5 dyn/cm^2)[7,17] and WSS < 1 dyn/cm^2 being representative of pathological flow conditions likely
89 found in occluded microvasculature[27,28]. Human brain microvascular endothelial cells (HBMECs) are
90 seeded into the network, and after 3 days in culture, they form fully endothelialised 3D microvessels (**Fig.
91 1d**). To experimentally model clinical malarial fever episodes, we exposed our engineered 3D human brain
92 microvessel system to 40 °C for 1 hour prior to iRBC perfusion, mimicking the hyperthermic episodes
93 observed in paediatric CM. Since increased temperature affects medium viscosity and density, WSS profiles
94 were simulated at both normothermic (37 °C) and febrile (40 °C) temperatures, showing minimal
95 differences (**Extended Data Fig. 1a**). After incubation of microvessels for 1 hour at either 37 °C or 40 °C,

96 normothermic *P. falciparum*-iRBC were perfused for 30 minutes at the same temperature as the vessel
97 incubation (**Fig. 1e**). Binding was quantified along the outer edges of the microvascular grid, and
98 fluorescent areas containing cytoadhered *P. falciparum*-iRBC were defined as the sequestered area
99 (**Extended Data Fig. 1b**). Multiple clonal lines of *P. falciparum*-iRBCs expressing predominantly single
100 PfEMP1 variants (**Extended Data Fig 2a-b**), including HB3var03 (EPCR-ICAM-1 binder), IT4var19
101 (EPCR binder), and IT4var31 (CD36-ICAM-1 binder), exhibited significantly increased binding at 40 °C
102 across multiple WSS conditions (**Fig. 1f-h**). Temperature did not affect uninfected RBC binding, which
103 remained negligiblele (**Extended Data Fig. 3**). At febrile temperature, ICAM-1 binders (HB3var03 and
104 IT4var31) presented increased binding across all WSS demonstrated, while the EPCR binder (IT4var19)
105 showed increased binding only at higher WSS (>1 dyn/cm²). As a negative control, we used a CSA-binding
106 line expressing var2csa, which mediates placental sequestration. NF54var2csa showed minimal binding at
107 37 °C and no changes at 40 °C, indicating that increased iRBC binding at fever-range temperatures occurred
108 in parasite lines that presented tropism for the brain endothelium (**Fig. 1i**). No significant temperature-
109 dependent changes were observed in endothelial junction organisation, microvessel diameter, endothelial
110 cell area, perimeter, or circularity, except for a slight non-signigicant increase in intracellular von
111 Willebrand Factor (vWF) mean fluorescence intensity (MFI), ruling out major heat-induced vessel
112 remodelling (**Extended Data Fig. 4a-f**). Together, these data show that febrile temperature promotes *P.*
113 *falciparum*-iRBC binding to endothelial cells in a PfEMP1- and flow-dependent manner.

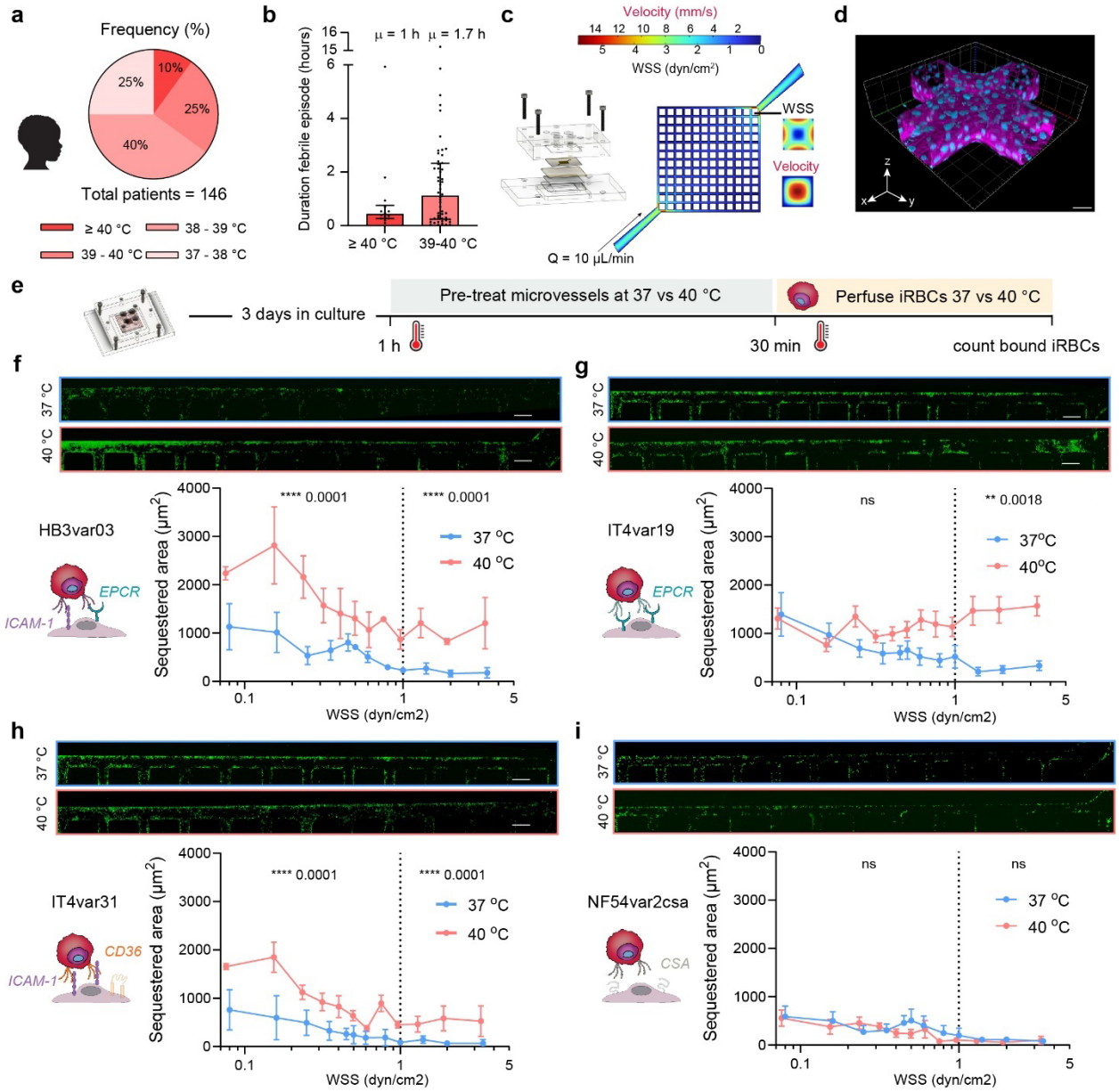

Fig. 1. Fever quantification in paediatric malaria patients and *P. falciparum*-iRBC binding at 37 and 40 °C to 3D microvessels. a, Distribution of maximum body temperature data during admission from 146 paediatric malaria cases in Zambia and Malawi treated with antipyretics as described in Methods. **b,** Duration of high fever episodes ≥ 40 °C or between 39 and 40 °C. Bar plot represent median and interquartile range; μ indicates group mean. **c,** Simulated mid-plane flow velocity in the grid network prior to collagen remodelling by HBMECs (see Methods). Inset: lumen cross-section velocity and WSS at first branch (black line).**d,** Volumetric reconstruction of a microvessel network grid cross section labelled with VE-cadherin antibody (magenta) and nuclear staining by DAPI (blue). Scale bar = 50 μm. **e,** Schematic representation of the binding assay workflow. **f-i,** Receptor binding schematic and iRBC sequestered areas at 37 °C and 40 °C across WSS for: f, HB3var03; g, IT4var19; h, IT4var31; i, NF54var2csa. Medians are represented by dots and interquartile range by error bars. Statistical analysis of binned regions (< 1 dyn/cm^2 and ≥ 1 dyn/cm^2) (dotted line) was determined by Mann-Whitney U test (n = 6 independent biological replicates for HB3var03, IT4var19, and IT4var31; n = 4 for NF54var2csa). Scale bars = 200 μm.

128 **EPCR and ICAM-1 mediate temperature-driven iRBC and neutrophil binding without changes in**
129 **receptor expression**

130 To investigate whether endothelial receptors are responsible for the mechanism underlying increased
131 sequestration at 40 ºC, we inhibited *P. falciparum*-iRBC binding using anti-ICAM-1 and anti-EPCR
132 antibodies. Systematic inhibition of ICAM-1, EPCR, or both at 40 ºC significantly reduced binding of both
133 *P. falciparum* lines HB3var03 and IT4var19 compared to an IgG control. Cytoadhesion at 37 and 40 °C did
134 not present any statistical difference after antibody treatment, reaching a baseline residual non-specific
135 binding, specially under pathological low flow (WSS < 1 dyn/cm²) (**Fig. 2a,b, Extended Data Fig. 5a-d**).
136 To examine the broader implications of febrile temperature-induced changes in vascular adhesion, we
137 perfused neutrophils into microvessels pre-incubated at either 37 °C or 40 ºC, known to bind to the
138 endothelium in an ICAM-1-mediated manner. Indeed, exposure to 40 ºC significantly increased
139 cytoadhesion of neutrophils at pathological low flow but not at higher WSS (**Fig. 2c**).
140 To determine whether a temperature-induced increase in expression of ICAM-1 or EPCR contributed to the
141 increase binding of *P. falciparum*-iRBC and neutrophils, we assessed total endothelial proteins by
142 employing quantitative mass spectrometry using tandem mass tag (TMT) labelling. Whole-proteome
143 analysis of HBMEC monolayers exposed to 40 °C for 1 hour revealed minimal changes in protein
144 expression (**Figure 2d**), with only a handful of significantly upregulated proteins (e.g., SFSWAP, UQCC1,
145 DPP9) and one downregulated transcript (SNRPD3). These proteins are primarily associated with RNA
146 splicing, mitochondrial function, or inflammasome regulation, while protein levels of EPCR and ICAM-1
147 remained unchanged. Although 1h exposure is probably insufficient for substantial changes at the protein
148 level, further analysis revealed slight increases in heparanase (HSPE), heat shock proteins (HSPs), and
149 prostaglandin synthesis pathway enzimes (PTGs), suggesting early fever-mediated endothelial stress and
150 initiation of heparan sulfate shedding (**Extended Data Fig.6**). We next used flow cytometry to quantify
151 both the surface levels and the proportion of cells expressing ICAM-1 and EPCR after heat (**Figure 2e,**
152 **Extended Data Fig. 7**). No differences were observed for ICAM-1, EPCR, or CD36, the latter being
153 minimally expressed in the brain. Maintenance of CD31 expression at 40 °C confirms endothelial cell
154 viability at febrile temperature (**Figure 2e, Extended Data Fig. 7**). Altogether, *P. falciparum*-iRBC binding
155 at 40 ºC is mediated by ICAM-1 and EPCR, however such increase is not explained by differences in the
156 receptor surface expression.
157

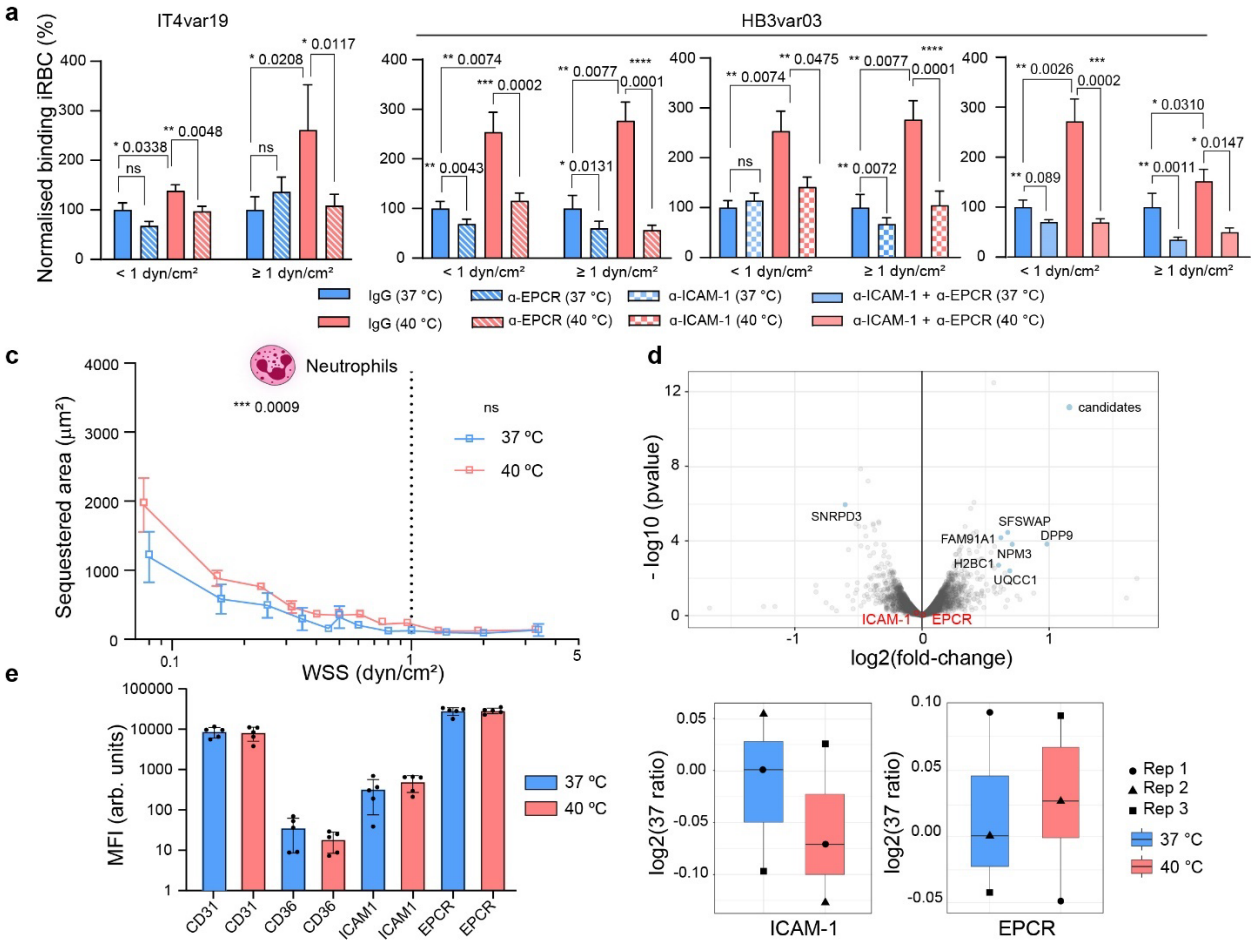

Fig. 2. Quantification of the role of endothelial receptors EPCR and ICAM-1 and neutrophil binding. **a,** Binding of the IT4var19 line at 37 °C or 40 °C in the presence of IgG isotype control (filled) or anti-EPCR mAb 252 antibody (stripes). **b**, Binding of the HB3var03 line at 37 °C or 40 °C in the presence of IgG isotype control (filled), anti-EPCR mAb 252 (stripes), anti-ICAM-1 mAb 15.2 (squares), and both (light colour). Percentage of binding for each treatment is normalised to the respective IgG control at 37 °C. Bars represent mean ± SEM. Statistical analysis for the two WSS regions WSS <1 dyn/cm² and WSS ≥ 1 dyn/cm² using Mann-Whitney U test; n= 4-6 independent microvessels. Stratified data can be found in Extended Fig. 5. **c,** Sequestered neutrophil area at 37 °C and 40 °C across WSS (medians as lines and interquartile ranges as error bars). Statistical analysis for the two WSS regions WSS <1 dyn/cm² and WSS ≥ 1 dyn/cm² using Mann-Whitney U test; n = 4 biological replicates per condition. **d,** Volcano plot of differential protein expression of HBMEC monolayer exposed to 37 °C or 40 °C for 1 h (top), with labeled candidates showing statistically significant changes in protein expression. ICAM1 and EPCR differential protein expression (bottom). *n* = 3 independent biological replicates. **e**, MFI of HBMEC surface level expression by flow cytometry after 1h at 37 °C and 40 °C. Bars represent mean ± standard deviation (SD) (n = 5-6 biological replicates).

Febrile temperature promotes endothelial glycocalyx shedding

The glycocalyx is a carbohydrate-rich layer that limits endothelial receptor accessibility[29,30]. To test whether febrile temperature disrupts the endothelial glycocalyx, we exposed HBMECs to 40 °C. Staining revealed a marked loss of sialic acids (**Fig. 3a**), heparan sulfate (**Fig. 3b**), and syndecan-4 (**Fig. 3c**). Syndecan-4, the

179 most abundant proteoglycan, also showed significant shedding (**Fig. 3d**). The decrease in glycocalyx
180 molecules was comparable to that induced by neuraminidase (NA) treatment, which cleaves terminal sialic
181 acid residues from membrane glycoproteins[31]. To determine if temperature-induced glycocalyx shedding
182 occurs in the vasculature of other organs, we fabricated microvessels from primary human pulmonary artery
183 endothelial cells (HPAECs), an important site of iRBC cytoadhesion[32,33]. Following 40 °C incubation, lung
184 microvessels displayed increased shedding of syndecan-1 (**Fig. 3e**), a marker of lung vasculature pathology
185 in malaria[34,35] and other microbial infections[36]. This was accompanied by a decrease in sialic acid but not
186 of heparan sulfate, similar to NA treatment (**Fig. 3f, g, Extended Data Fig. 8a, b**).
187 To determine whether glycocalyx degradation is responsible for enhanced *P. falciparum*-iRBC binding, we
188 pretreated 3D brain microvessels with NA for 30 minutes at 37 °C, followed by perfusion with HB3var03
189 and IT4var19 *P. falciparum*-iRBCs. Binding doubled at WSS < 1 dyn/cm² for both lines, reaching levels
190 similar to those observed at 40 °C (**Fig. 4h, i**). However, NA treatment failed to reproduce increased binding
191 observed at WSS ≥ 1 dyn/cm², specially for the EPCR binder, IT4var19 (**Fig. 4i**). Incubation with anti-
192 EPCR and ICAM-1 inhibitory antibodies in combination with NA treatment, brought *P. falciparum*-iRBC
193 binding levels back to baseline, thus confirming enhanced PfEMP1-receptor interactions upon glycocalyx
194 disruption (**Extended Data Fig. 9a, b**). These findings support a model in which fever-induced
195 temperatures promote the shedding of sialic acids and other glycan structures, thereby facilitating PfEMP1-
196 mediated adhesion predominantly under low WSS.

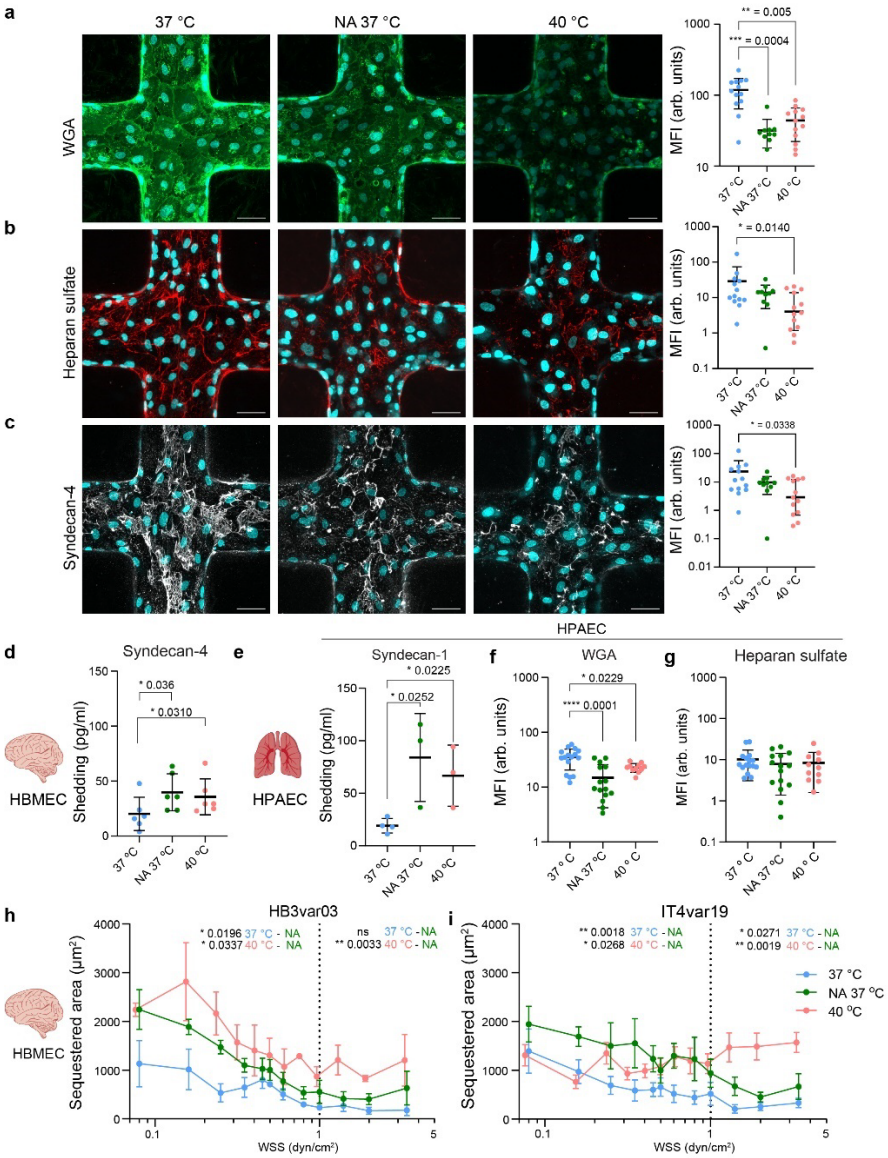

Fig. 3. Quantification of endothelial glycocalyx shedding. Immunofluorescence z-stack of microvessel cross sections (left) and MFI normalised by number of cells quantified by DAPI (left) of **a**, sialic acids labelled with FITC-conjugated Wheat Germ Agglutinin (WGA), **b,** heparan sulfate and **c**, syndecan-4; dot plots (right) show mean ± SD, n = 4 microvessels per condition, each dot is a region of interest. Scale bars: 50 µm. **d,** Syndecan-4 shedding quantified by ELISA of 3D brain microvessel supernatants following exposure to 37 °C or 40 °C. **e**, Syndecan-1 shedding quantified by ELISA of 3D pulmonary microvessel supernatants. Graphs show mean ± SD, in which each dot is from a different microvessel batch. Immunofluorescence MFI quantification of **f**, sialic acids labelled with WGA, and **g**, heparan sulfate in 3D pulmonary microvessels; box plot show mean ± SD, n = 4 microvessels per condition, each dots is a region of interest. Conditions in **a-g** include 37 °C or 40 °C incubation for 1 hour, and NA treatment for 30 min at 37 °C (1 U/mL). Statistical analysis was done by one-way ANOVA with Tukey's multiple comparisons or pairwise comparisons were performed using the two-sided Mann-Whitney U test. **h-i)** HB3var03 and IT4var19 binding to 3D brain microvessels treated with NA (n = 5 microvessels) compared to 37 °C and 40 °C (n = 6 microvessels). Medians are shown as dots; error bars represent interquartile range. Statistical analysis by Kruskal-Wallis test for binned WSS regions (< 1 dyn/cm² vs ≥ 1 dyn/cm²; dotted line).

213 **Matrix metalloproteinase inhibition preserves the glycocalyx and reverses temperature-induced**
214 **cytoadhesion**

215 To investigate the mechanisms driving glycocalyx degradation at febrile temperature, we analysed the
216 secretion of angiogenic mediators, inflammatory cytokines, proteolytic enzymes, and endothelial markers
217 from HBMEC monolayers using a semi-quantitative protein array. After 1 hour at 40 °C, HBMEC exhibited
218 significantly increased secretion of extracellular matrix remodelling proteases, such as matrix
219 metalloproteinase-1 (MMP-1) and vascular inflammatory markers including angiopoietin-2 (ANGPT2). No
220 significant increases in pro-inflammatory cytokines IL-6, IL-1 β, and TNF-α, were observed after 1 hour at
221 40 °C (**Fig. 4a**). As MMP-1 has been shown to be linked to glycocalyx degradation[37], we next examined
222 whether the broad MMP inhibitor batimastat reverses enhanced iRBC cytoadhesion. Indeed, binding of
223 both HB3var03 and IT4var19 *P. falciparum*-iRBCs at 40 °C was significantly reduced by microvessel
224 batimastat pre-treatment at both healthy and pathological WSS, with sequestration levels comparable to
225 those at 37 °C (**Fig. 4b, c**). Furthermore, we confirmed that batimastat stabilised the glycocalyx, preventing
226 sialic acid, heparan sulfate, and syndecan-4 removal at 40 °C (**Fig. 4d-f**). Altogether, our results show that
227 short-term exposure of endothelial cells to febrile temperatures promotes iRBC binding by MMP-mediated
228 glycocalyx breakdown, and suggests that protection of the glycocalyx could be a potential therapeutic
229 avenue in the prevention of iRBC cytoadhesion during severe malaria.

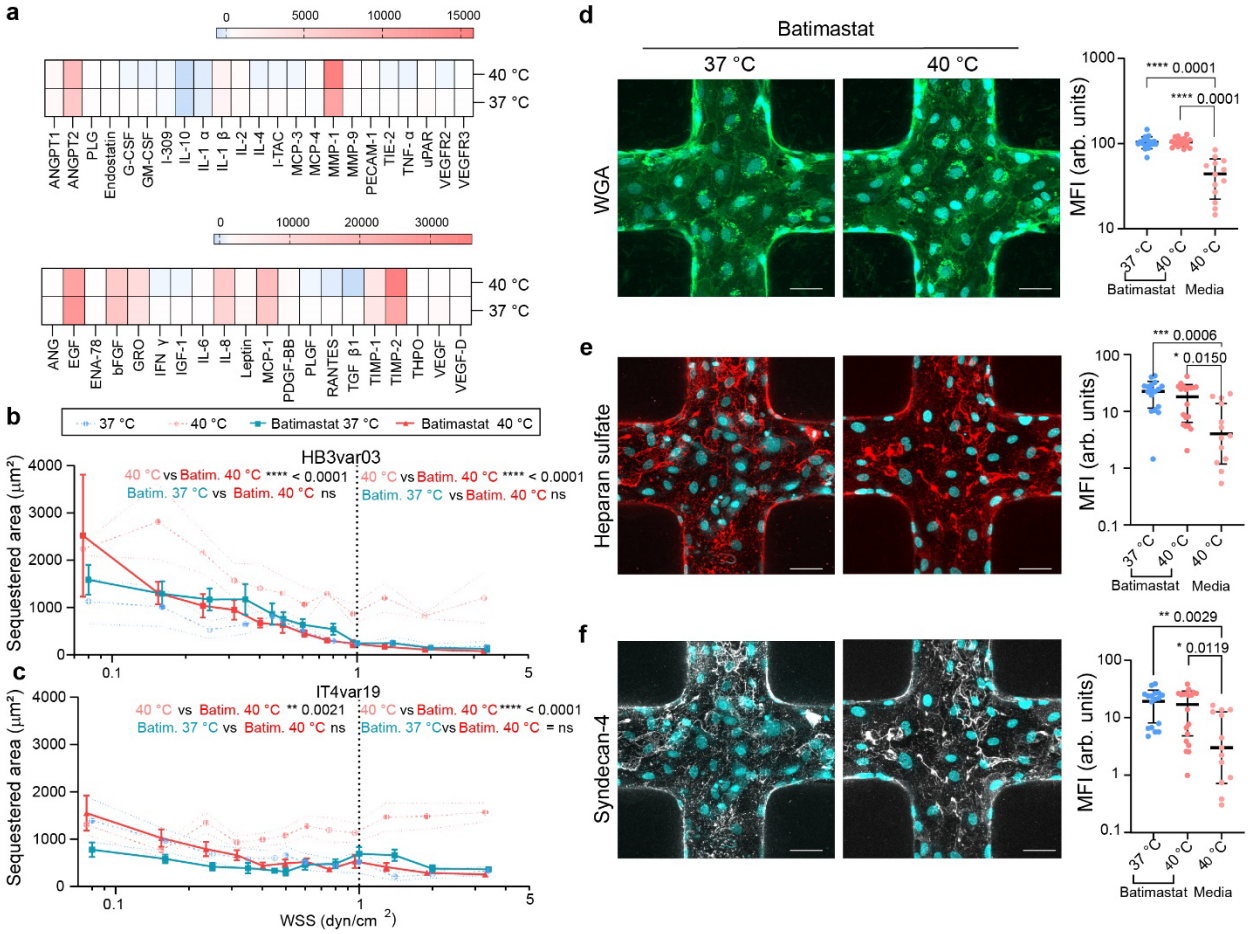

Fig. 4. Analysis of protective effect by batimastat, an MMP inhibitor a, Quantification of angiogenesis-related molecule secretion from HBMEC monolayers after 1 h at 37 °C or 40 °C. Supernatants pooled from n=3 biological replicates and normalised as described in Methods. **b-c,** HB3var03 and IT4var19 binding after batimastat-treatment of 3D brain microvessels at 37 °C or 40 °C (n = 4 brain microvessels). Median ± error bars representing interquartile range. Statistical analysis by Kruskal-Wallis test for binned WSS regions (< 1 dyn/cm² vs ≥ 1 dyn/cm²; dotted line). **d-f,** Z-projection immunofluorescence images of batimastat pre-treated microvessels exposed to 37 °C or 40 °C and labelled for WGA, heparan sulfate, syndecan-4 and DAPI (cyan) (left) and measurement of the MFI normalised by number of cells using DAPI (right) (n = 4 brain microvessels, dots represent quanfied ROI). Statistical analysis by one-way ANOVA with Tukey's multiple comparisons; box plots show mean ± SD. Scale bars = 50 μm.

Discussion

Although fever generally exerts protective effects for the host against infection, our findings reveal that during severe malaria infection it may paradoxically amplify pathology by promoting cytoadhesion of *Plasmodium falciparum*–iRBCs. This study shows that brief exposure to high febrile temperatures causes glycocalyx shedding, increasing interactions with blood cells, including *Plasmodium falciparum*-iRBC and neutrophil cytoadhesion. Enhanced cytoadhesion has important clinical implications as elevated

248 sequestered parasite biomass in the microvasculature is a key component of severe malaria[38,39,14]. Increased
249 parasite adhesion during fever could directly worsen disease progression, by promoting vascular obstruction
250 and blood-brain barrier disruption through inflammatory and permeability-inducing pathways[40–43]. In
251 addition, neutrophil extracellular traps and neutrophil extravasation are linked to CM[44,45] and acute
252 respiratory distress syndrome[46], respectively. This aligns with clinical observations linking higher febrile
253 episodes to adverse outcomes, including epilepsy, long-term disabilities and cognitive impairments[47].

254 A key finding of this study is that febrile temperature promotes degradation of the endothelial glycocalyx.
255 The glycocalyx is a dynamic network of sugars and proteins lining the vascular endothelium, which forms
256 a barrier that limits direct interaction of endothelial cells with circulating blood cells and vascular
257 components. Its breakdown is common in severe *P. falciparum*[48–51], *vivax*, and *knowlesi* malaria[35], with
258 fever emerging as a unifying symptom across malaria infections, despite the three parasites presenting
259 significant differences in biology. Recovery of the glycocalyx is slow, requiring about 20 hours after
260 enzymatic degradation *in vitro*[52] and up to 7 days *in vivo*[53]. The glycocalyx varies in thickness from 0.2 to
261 4.5 μm[54], being more prominent in the brain than in the lung[55,56]. Major cytoadhesion receptors, such as the
262 ~18.7 nm[57,58] ICAM-1 and the even smaller EPCR, lie well beneath this layer. Our results show that short
263 episodes of fever degrade the brain and lung endothelial glycocalyx, exposing these normally shielded
264 receptors and thereby facilitating *P. falciparum*-iRBC and neutrophil binding under flow[29]. We confirmed
265 this by the enzymatic removal of terminal sialic acids with neuraminidase, which reproduced the febrile
266 binding phenotype under pathological flow conditions (WSS < 1 dyn/cm²) for both HB3var03 and
267 IT4var19. Neuraminidase mostly affects the outermost negative-charged glycocalyx layer. By contrast,
268 febrile-range temperatures induced shedding of deeper components, such as syndecan-4 and heparan
269 sulfate. This mechanistic distinction could explain why neuraminidase treatment alone failed to replicate
270 the full febrile binding profile at higher, physiological WSS (≥ 1 dyn/cm²), in which *P. falciparum*-iRBCs
271 are only exposed briefly to the endothelial surface.

272 Our study also shed light on the mechanism of temperature-dependent glycocalyx shedding. Although 1
273 hour incubation at 40 °C did not elicit a detectable increase in pro-inflammatory cytokines such as IL-6, IL-
274 1 β, IFN γ or TNF-α, or enhanced EPCR and ICAM-1 expression, hyperthermia triggered a rapid release
275 of MMP-1 and Angiopoietin-2, both implicated in glycocalyx breakdown[59] and CM pathology[60,61,62]. Both
276 molecules are stored in intracellular endothelial vesicles and can rapidly be released[63], contributing to
277 extracellular matrix remodelling and directly facilitating glycocalyx degradation[64]. Previous findings
278 suggest that temperature-induced MMP1 release could be further amplified by *P. falciparum*, as endothelial
279 cells upregulate MMP1–3 in response to iRBCs at elevated temperatures[65]. Additionally, expression of
280 heparanase, an endoglycosidase that cleaves heparan sulfate and plays a role in neutrophil adhesion during

281 sepsis[55], was increased following exposure to febrile temperatures. As MMPs can synergise with heparanase
282 to enhance its expression, this may provide an additional mechanism for temperature-dependent glycocalyx
283 breakdown[66]. Importantly, we demonstrated that the MMP inhibitor batimastat can prevent glycocalyx
284 shedding[67] and the temperature-dependent increase in binding to EPCR and ICAM-1, suggesting potential
285 therapeutic benefit, in agreement with previous mouse experimental cerebral malaria studies showing
286 delayed mortality[68]. However, batimastat's broad-spectrum activity, lack of specificity and off-target effects
287 limit its clinical development and suggest the use of more specific MMP inhibitors[69]. In the absence of
288 effective host-directed therapies for severe malaria, our findings underscore the need for aggressive
289 antipyretic treatment.

290 Beyond malaria, hyperthermia profoundly shapes vascular and immune interactions. It accelerates
291 neutrophil migration[70] and extracellular trap formation[71], enhances leukocyte adhesion[37,72–75], and promotes
292 MMP release in sepsis[76] and stroke[77], driving basement membrane breakdown. Glycocalyx dysregulation
293 is increasingly recognised as a central determinant of vascular vulnerability, implicated in viral lung
294 injury[30,78], sepsis[55], ageing and neurodegeneration[79]. Consistently, hyperthermia worsens outcomes in
295 stroke[9] and hypoxic–ischemic brain injury[80] by disrupting the blood–brain barrier and causing brain
296 edema[81] —paralleling CM pathology. Our findings therefore extend to a broader principle: febrile
297 temperature destabilises the glycocalyx and amplifies microvascular pathology across infectious and
298 inflammatory diseases.

299 Our flow-based microvessel chip overcomes the restrictions of traditional assays used to study the effects
300 on febrile temperatures on *P. falciparum*-iRBC interactions, that relied on recombinant proteins, which lack
301 glycans or protein ability to freely move and rearrange on the plasma membrane. For example,
302 discrepancies have been found when using force-spectroscopy to measure binding strength to recombinant
303 proteins, showing a weaker binding to recombinant receptors after heating [18,82], while binding studies with
304 iRBCs maintained increased cytoadhesion to cell lines[18]. The 3D platform has been previously validated in
305 studies of *P. falciparum* interactions with EPCR and ICAM-1[83], and in testing inhibitory effect of plasma[84]
306 or monoclonal antibodies[85]. An advantage of our system, is that it allows to decouple the temperature-effect
307 of fever, independently of elevated pro-inflammatory cytokine levels, key pyrogens that upregulates
308 endothelial receptors, such as ICAM-1. The independent tuning of physical and biological parameters also
309 represents and advantage over hyperthermia animal models. A plausible limitation that remains is that rapid
310 mechanical modifications at the surface of the *P. falciparum*-iRBC could further contribute to increased
311 cytoadhesion. However, the strong inhibition of binding with batimastat suggests that glycocalyx disruption
312 is a major responsible for increase binding. Future studies should examine the impact of glycocalyx
313 impairment on bond dynamics under flow, the combined effect of hyperthermia and inflammatory

signalling in malaria, and extend the model with additional blood–brain barrier cell types or immune cells to directly assess febrile contributions CM pathology.

Methods

Body temperature measurements in patients

Body temperature data were collected from 146 children (ages 2–11) who received the WHO recommended treatment with 15 mg/kg acetaminophen every 6 hours as needed for temperatures ≥ 38.5 °C. Participants were enrolled at Queen Elizabeth Central Hospital (Blantyre, Malawi), University Teaching Hospitals Children's Hospital (Lusaka, Zambia), and Chipata Central Hospital (Chipata, Zambia)[7,10]. All had *P. falciparum* infection confirmed by blood smear or rapid diagnostic test and presented with central nervous system symptoms (impaired consciousness and/or seizures) of whom 72–83% met CM criteria. Temperatures were recorded via a body patch every 2–4 minutes over a 72-hour period, during which most children defervesce. Ethics approvals: Biomedical Research Ethics Committee (Zambia): 003-06-18, University of Rochester Research Subjects Review Board: 00067717, and College of Medicine Research and Ethics Committee (Malawi): P.10/17/2298.

Primary cell culture and 3D brain microvessel fabrication

Primary human brain microvascular endothelial cells (HBMECs) (Cell Systems ACBRI 376) and primary human pulmonary artery endothelial cells (HPAECs) (Lonza CC-2530) were grown in a flask coated with poly-L-lysine (Sigma #P8920) up to passage 9 before they were seeded in microvessels. 3D microvessel devices were prepared as described previously[83]. The top part of the microvessels is generated by injecting type I collagen (7.5 mg/mL) into the space created between the top plexiglass jig and a polydimethylsiloxane (PDMS) mold with a 13-by-13 grid geometry, fabricated using soft lithography. The bottom part consists of a flat layer of collagen, compressed between a flat PDMS stamp and a 22-by-22 mm coverslip positioned on the bottom jig. After 30 minutes of gelation at 37 °C, the PDMS stamps were removed, and the top and bottom jigs were sealed creating a three-dimensional network within the collagen hydrogel. Primary HBMECs or HPAECs were seeded at a concentration of $7x10^6$ cells/mL under gravity-driven flow by adding 8 µL volume increments to the device inlet until reaching full coverage in the microfluidic network. Microvessels were then cultured for up to 3 days and fed every 12 hours by gravity-driven flow before performing *P. falciparum* binding experiments.

Numerical simulation of wall shear stress rates

344 The flow characteristics of 3D brain microvessels were simulated using COMSOL Multiphysics software,
345 as previously described[83]. Flow in the microvessel network (diameter 120 µm) was assumed to be laminar,
346 and the stationary solver for laminar flow was used with predefined Navier-Stokes equations. Due to the
347 low hematocrit (<0.1%) used during perfusion, flow was assumed to be Newtonian, and wall shear stress
348 (WSS) rates were calculated based on fluid viscosity of water or culture medium at 37 °C (viscosity of
349 6.922×10^{-4} Pa s and density of 993.3 kg/m^3) and 40 °C (viscosity of 6.539×10^{-4} Pa s and density of
350 992.2 kg/m^3). The inlet boundary conditions were defined for the perfusion flow rate of 10 µl/min, and the
351 outlet boundary conditions were set at zero pressure.

352 *Plasmodium falciparum culture*

353 *P. falciparum* lines HB3VAR03, IT4VAR19, and IT4var31 were cultured in human O+ erythrocytes in
354 RPMI-1640 medium (Gibco) containing 25 mM HEPES, 1.5 g/L gentamicin, 0.4 mM hypoxanthine, 26.8
355 mM sodium bicarbonate, 5 mM glucose, and 10% human type AB+ serum (complete RPMI). Parasites
356 were grown in a gas mixture of 90% N2, 5% CO2, and 5% O2 and parasitemia and daily checked by Giemsa
357 staining. Cultures were regularly panned and monitored for correct PfEMP1 expression on primary
358 HBMECs. *P. falciparum* parasites were synchronized weekly using 5% sorbitol to select for ring-stage
359 parasites.

360 *Temperature-dependent P. falciparum-iRBC and neutrophil binding assay in 3D brain*
361 *microvessels*

362 *P. falciparum* cultures were enriched for mature-stage iRBCs using a MACS cell separator with LD columns
363 (Miltenyi Biotec 130-042-901) and diluted to 5×10^6/mL in complete RPMI. The iRBCs were labeled with
364 the membrane dye PKH26 Red Fluorescent Cell Linker Midi Kit (Sigma MIDI26-1KT) according to
365 manufacturer's instructions. For neutrophil binding experiments, neutrophils were isolated from whole
366 blood samples, obtained from the Catalan Blood and Tissue Bank, using the EasySep Direct Human
367 Neutrophil Isolation kit (StemCell 19666) according to manufacturer's instructions. Isolated neutrophils
368 were labeled with the membrane dye PKH26 and resuspended to a concentration of 2 x 10^6 neutrophils/mL
369 in RPMI 1640 (Sigma) supplemented with 5% heat-inactivated fetal bovine serum (Gibco), 0.1% vascular
370 endothelial growth factor (Lonza), 0.4% recombinant human FGF (Lonza), 0.1% ascorbic acid (Lonza),
371 0.1% R3-insulin-like growth factor (Lonza), 0. 1% recombinant human endothelial growth factor (Lonza),
372 0.5% penicillin/streptomycin (Gibco) and 1% Glutamax (Gibco). The 3D brain microvessels were pre-
373 incubated for 1 hour at either 37 °C or 40 °C. before normothermic iRBCs or neutrophils were perfused for
374 30 min at 37 °C or 40 °C, respectively, at a flow rate of 10 µl/min using a syringe infusion pump (KD
375 Scientific KDS220). After perfusion, a 5-minute wash with EGM-2MV endothelial medium followed at the

same flow rate. Microvessels were fixed in 4% PFA for 20 minutes followed by two 10-minute washes in PBS, and stained with DAPI (8 µg/mL). Each 3D microvessel device was used once for each experimental condition. For *P. falciparum*-iRBC binding inhibition experiments with blocking antibodies, microvessels were pretreated for 20 min at the respective temperature with mouse anti-human ICAM-1 monoclonal antibody (mAb) 15.2 (Abcam; ab20 [5 µg/ml]), rat anti-human EPCR mAb 252 (Sigma-Aldrich; E6280-200UL [50 µg/ml]), or mouse (Abcam; ab19443) or rat (Thermo Fisher; 14-4301-85) IgG isotype control before perfusing iRBCs by gravity-driven flow. For drug inhibition experiments, microvessels were pretreated with the MMP inhibitor batimastat (R&D systems; 2961) at 5µM for 2-h prior to the 1-h incubation at 37 °C or 40 °C.

P. falciparum-iRBC and neutrophil binding quantification

For each device, the edges of the 13-by-13 grid were imaged. A Zeiss LSM 980 AiryScan2 microscope with 10× NA 0.3 objective was used to image cytoadhered iRBCs or neutrophils labeled with PKH26 membrane dye (laser 555 nm) and DAPI-stained parasite and HBMEC nuclei (405 nm laser). DAPI staining was used as control to confirm that HBMEC coverage of the microvessels was uniform. Images were acquired at a 3-µm Z-step size, and projection images of the bottom of the vessel were produced from Z-stacks using Fiji (ImageJ v1.52b) software. The cytoadhered area indicates the area occupied by attached iRBCs across the 12 predefined regions along the edges of the device, as described previously[85]. To minimize flow artifacts, parasite binding was assessed exclusively in the central region of the channel, where flow remains laminar and fully developed, avoiding junctions between branches. Entry and exit regions were excluded, as flow is not fully developed in these regions. Each edge was considered a technical replicate for each device, while each device was considered an independent biological replicate. For statistical analysis, WSS range was divided into 2 regions named pathological[27,28] (<1 dyn/cm²) and physiological (≥1 dyn/cm²)[83,86], in line with flow values observed in postcapillary venules under healthy versus inflammatory conditions.

Immunofluorescence microscopy of 3D microvessels

Fixed 3D brain microvessels were incubated in Background Buster (Innovex #NB306) for 30 minutes and blocking buffer (2% bovine serum albumin, 0.1% Triton X-100 in PBS) for 1 hour. Blocked microvessels were stained overnight at 4 °C with mouse anti-VE-cadherin primary antibody (Abcam, ab33168) and sheep anti-vWF (Bio-Rad, AHP062) at 1:100 dilution. For Glycocalyx staining, microvessels were blocked with 2% bovine serum albumin in PBS for l hour and stained overnight at 4 °C with 1:50 Human anti-Syndecan-4 antibody (R&D Systems, AF2918-S) and 1:100 anti-Heparan Sulfate (Amsbiom, 370255-S). Microvessels were washed six times for 10 minutes with PBS and incubated for 1 hour at RT with 1:250 Alexa-Fluor 488-, Alexa-Fluor 594- or Alexa-Fluor 647-conjugated secondary antibodies (Invitrogen),

408 containing DAPI 2 μg/mL (ThermoFisher, D21490; 1:250). Following secondary antibody incubation,
409 glycocalyx-stained microvessels were labeled with FITC-conjugated Wheat Germ Agglutinin WGA (VWR
410 29022-1/ 29022-1; 1:50) for 20 minutes at RT. Microvessels were then washed six times for 10 minutes
411 with PBS and imaging was done using a Zeiss LSM 980 AiryScan 2 confocal microscope with a 20× NA
412 0.8 objective using a 1-μm Z-step. The 3D rendering of a microvessel cross-section shown in **Fig. 1** was
413 obtained using Zeiss ZEN v3.3 and Arivis Vision4D v3.5.1 software.

414 *Human Cytokine Antibody Array*

415 For cytokine analysis, supernatants were collected from 2D HBMEC monolayers grown in 6-well plates
416 from n = 3 biological replicates. A human angiogenesis array (Abcam, ab193655) was performed according
417 to the manufacturer's instructions. The relative expression of cytokines (measured by chemiluminescence
418 intensity) was compared between samples exposed to 37 °C and 40 °C for 1 hour, corrected to the negative
419 controls on each array, and normalised to the positive controls as suggested by the kit manufacturer. The
420 blots were visualised and imaged (1 min exposure) using the Fusion FX Spectra (Vilber, France).

421 *ELISA assay*

422 Media from the outlet reservoir of each device was collected after incubation for 1 hour at 37 °C and 40 °C
423 from N = 3-6 experiments at day 3. Quantification of Syndecan-4 and Syndecan-1 was performed using the
424 Human Syndecan-4 DuoSet ELISA kit (R&D Systems, DY2918) and Human Syndecan-1 DuoSet ELISA
425 kit (R&D Systems, DY2780), according to manufacturer's instructions.

426 *Proteomics*

427 Sample Preparation: HBMEC cells were cultured on flasks for three to four days until confluent, and then
428 incubated for 1 h either at 37 °C or 40 °C (total of 3 biological replicates per condition). Cells were lysed
429 in cold RIPA buffer with 1× protease inhibitors, incubated on ice for 15 min, sonicated (5 pulses of 5 min
430 at 0/0.5 high, 5°C), and centrifuged at ~14,000 × g for 15 min. Protein concentration was determined using
431 the BCA assay by incubating 20 μL of samples with 200 μL of BCA working reagent (50:1, Reagent A:B)
432 at 37°C for 30 min, followed by absorbance measurement at 562 nm. Samples were subjected to the SP3
433 protocol[87,88] on a King Fisher Apex Platform (Thermo Fisher) and peptides were eluted by tryptic digestion
434 (sequencing grade trypsin, Promega) for 5 h at 37°C. Peptides were labelled with TMT6plex[89] Isobaric
435 Label Reagent (ThermoFisher) according the manufacturer's instructions. In short, 0.8 mg reagent was
436 dissolved in 42 μL acetonitrile (100%) and 4 μL of stock was added and incubated for 1h room temperature.
437 Followed by quenching the reaction with 5% hydroxylamine for 15 min at RT. Samples were combined and
438 for further sample clean up an OASIS® HLB μElution Plate (Waters) was used. The TMT6-labelled
439 proteome was fractionated by high-pH reversed-phase carried out on an Agilent 1200 Infinity high-

440 performance liquid chromatography system, equipped with a Gemini C18 column (3 µm, 110 Å, 100 x 1.0
441 mm, Phenomenex). 48 fractions were collected along with the LC separation that were subsequently pooled
442 into 12 fractions. Pooled fractions were dried under vacuum centrifugation and reconstituted in 10 µL 1%
443 formic acid, 4% acetonitrile and then stored at -80 °C until LC-MS analysis.

444 Data acquisition. Samples were measured on an Q Exactive™ Mass Spectrometer (Thermo) coupled to an
445 UltiMate 3000 RSLC nano LC system (Dionex). Sample was concentrated on a C18 µ-Precolumn (Acclaim
446 PepMap 100, 5µm, 300 µm i.d. x 5 mm, 100 Å) and resolved on a nanoEase™ M/Z HSS T3 column from
447 Waters (75 µm x 250 mm C18, 1.8 µm, 100 Å). Trapping was carried out at a constant flowrate of 30
448 µL/min 0.5% trifluoroacetic acid in water for 4 min. Subsequently, peptides were eluted via the analytical
449 column (solvent A: 0.1% formic acid in water, 3% DMSO) with a constant flow of 0.3 µL/min, with
450 increasing percentage of solvent B (0.1% formic acid in acetonitrile, 3% DMSO) from 2% to 8% in 6 min,
451 8% to 28% in 37 min, from 28% to 40% in 9 min, followed by an increase of B from 40-80% for 3 min and
452 a re-equilibration back to 2% B for 5 min. The peptides were introduced into the mass spectrometer via a
453 Pico-Tip Emitter 360 µm OD x 20 µm ID; 10 µm tip (New Objective) and an applied spray voltage of 2.4
454 kV. The capillary temperature was at 275°C. Settings for the Q Exactive were: Full mass scan (MS1) was
455 acquired with mass range 375-1200 m/z, profile mode, in the orbitrap, resolution of 70000, fill time 10 ms.
456 AGC target 3E6. Data dependent acquisition (DDA) was performed with the resolution of the Orbitrap set
457 to 17500, fill time 50 ms, AGC target of 9E1 ions. Normalized collision energy of 32, HCD, fixed first mass
458 110 m/z.

459 Database search. Fragpipe v21.1 with MSFragger v4.0[90] was used to process the acquired data, which was
460 searched against the homo sapiens Uniprot proteome database (UP000005640, ID9606, 20594 entries,
461 release October 2022) with common contaminants and reversed sequences included. The following
462 modifications were considered as fixed modification: Carbamidomethyl (C) and TMT6 (K). As variable
463 modifications: Acetyl (Protein N-term), Oxidation (M) and TMT6 (N-term). For the MS1 and MS2 scans a
464 mass error tolerance of 20 ppm was set. Further parameters were: Trypsin as protease with an allowance of
465 maximum two missed cleavages; Minimum peptide length of seven amino acids; The false discovery rate
466 on peptide and protein level was set to 0.01.

467 Data analysis. The raw output files of FragPipe (protein.tsv files) were processed using the R programming
468 environment (ISBN 3-900051-07-0). Initial data processing included filtering out contaminants and reverse
469 proteins. Only proteins quantified with at least 2 razor peptides (with Razor.Peptides >= 2) were considered
470 for further analysis. 4203 proteins passed the quality control filters. In order to correct for technical
471 variability, batch effects were removed using the 'removeBatchEffect' function of the limma package on the
472 log2 transformed raw TMT reporter ion intensities ('channel' columns)[91]. Subsequently, normalization was

473 performed using the 'normalizeVSN' function of the limma package (VSN - variance stabilization
474 normalization[92]). Differential expression analysis was performed using the moderated t-test provided by the
475 limma package[91]. The model accounted for replicate information by including it as a factor in the design
476 matrix passed to the 'lmFit' function. Proteins were annotated as hits if they had a false discovery rate (FDR)
477 below 0.05 and an absolute fold change greater than 2. Proteins were considered candidates if they had an
478 FDR below 0.2 and an absolute fold change greater than 1.5.

479 *Flow cytometry*

480 HBMECs were cultured in flasks for 3–4 days until confluent, then transferred to 6-well plates and
481 incubated for 1 h at either 37 °C or 40 °C. Cells were rinsed with HBSS and detached using 15 mM EDTA
482 in HBSS. A total of 1×10^5 cells were seeded into wells of a 96-well plate and washed once with PBS
483 containing 0.5% BSA at room temperature. Antibody staining was performed on ice, with each step
484 incubated for 30 minutes. The following antibodies were used: goat anti-human EPCR (5 µg/ml; R&D
485 Systems, AF2245), followed by donkey anti-goat Alexa Fluor 647-conjugated secondary antibody (1:400;
486 Invitrogen, A32849); PE-conjugated anti-human ICAM-1 (2 µl per 10^6 cells; Miltenyi Biotec, REA266,
487 130-120-711) and relative isotype control PE-conjugated human IgG1 (Miltenyi, 130-113-471); FITC-
488 conjugated anti-human CD31 (5 µl per 10^5 cells; BD Pharmingen, 560984) and relative FITC-labelled
489 mouse IgG1 (Abcam, ab18447); FITC-labelled anti-human CD36 (10 µl per 10^5 cells; Abcam, ab39022)
490 and relative FITC-conjugated mouse IgG1 isotype control (2 µg/ml; Abcam, ab106163).
491 Phosphatidylserine (PS)-exposing apoptotic cells were identified using Annexin V mouse anti-human
492 (10 µg/ml; CoraLite 647, Proteintech, 1E6A8) in Annexin V Binding Buffer. All experiments were
493 performed on live cells, and dead cells were excluded using DAPI (ThermoFisher, D21490; 1:600 dilution).
494 The percentage of positive gated cells and mean fluorescence intensity (MFI) were quantified. Data were
495 analysed using FlowJo v10 software (Tree Star Inc.).

496 *Statistical analysis*

497 GraphPad Prism (version 10.2.0) was used for statistical analysis. For normally distributed samples,
498 pairwise comparisons were analysed by unpaired t-test with Welch's correction, while for non-normally
499 distributed samples using Mann-Whitney U test. To compare multiple conditions of normally or non-
500 normally distributed samples we used Kruskal-Wallis test with Dunn's multiple comparisons test and one-
501 way ANOVA with Tukey's multiple comparisons, respectively. P values < 0.05 were considered statistically
502 significant. Values are reported as median (Interquartile Interval), mean ± standard deviation or standard
503 deviation of the mean when indicated. Statistical significance is reported as: $*p < 0.05$, $**p < 0.01$, $***p$
504 < 0.001, $****p < 0.0001$. Parasite binding conditions with low variability were tested in four independent
505 3D microvessel devices, while conditions with high variability were tested in 6 independent devices.

506 **Data availability**

507 The mass spectrometry proteomics data have been deposited to the ProteomeXchange Consortium via the
508 PRIDE [1] partner repository with the dataset identifier PXD063878.

509

510 **Acknowledgements**

511 The authors thank Jennifer Schwarz and the Proteomics Core Facility at EMBL Heidelberg, the CRG-UPF
512 Flow cytometry facility, Alina Batzilla for experimental advice and Moritz Treeck for sharing the
513 NF54DiCre parasite line. The great majority of this work was funded by the European Research Council
514 (ERC) under the European Union's Horizon 2020 research and innovation program (Grant agreement no.
515 948088), the EMBL core program funding and contributions from the EMBL Infection Biology Transversal
516 Theme (Transition to Independence Grant to VI). VI was supported by a Marie Skłodowska-Curie Actions
517 post-doctoral fellowship FEBRIS [101026717]), and ORO by the EIPOD-LinC fellowship program, funded
518 by EMBL Marie Skłodowska Curie Actions. FS was supported by the Proteomics Core Facility at EMBL
519 Heidelberg. Patient FEVER study was carried out by GLB and KBS and supported by the NIH grants
520 R01NS102176 and R35NS122265.

521 **Authorship contributions**

522 Conceptualization: VI, MB; Methodology & validation: VI, RKML, MB; Data collection: VI, RKML,
523 ORO, LH, SSS, GMH, BLG, KBS, GLB; Data analysis: VI, RKLM, ORO, MGM, LH, FS; Visualization:
524 VI, MB; Writing original draft: VI, RKML, MB; Supervision: MB; Project Administration: VI, MB;
525 Funding Acquisition: VI, MB; All authors gave final approval for publication.

526 **Competing interests**

527 The authors declare no competing interests.

528

529 **References**

530 1. Yamagata, K. *et al.* Coexpression of Microsomal-Type Prostaglandin E Synthase with
531 Cyclooxygenase-2 in Brain Endothelial Cells of Rats during Endotoxin-Induced Fever. *J Neurosci* **21**,
532 2669–2677 (2001).
533 2. Eskilsson, A. *et al.* Immune-Induced Fever Is Dependent on Local But Not Generalized Prostaglandin
534 E2 Synthesis in the Brain. *J. Neurosci.* **37**, 5035–5044 (2017).
535 3. Lazarus, M. *et al.* EP3 prostaglandin receptors in the median preoptic nucleus are critical for fever
536 responses. *Nat Neurosci* **10**, 1131–1133 (2007).
537 4. Evans, S. S., Repasky, E. A. & Fisher, D. T. Fever and the thermal regulation of immunity: the
538 immune system feels the heat. *Nat Rev Immunol* **15**, 335–349 (2015).
539 5. Launey, Y., Nesseler, N., Mallédant, Y. & Seguin, P. Clinical review: fever in septic ICU patients--
540 friend or foe? *Crit Care* **15**, 222 (2011).
541 6. Polderman, K. H. Induced hypothermia and fever control for prevention and treatment of
542 neurological injuries. *Lancet* **371**, 1955–1969 (2008).
543 7. Chilombe, M. B. *et al.* Aggressive antipyretics in central nervous system malaria: Study protocol of a
544 randomized-controlled trial assessing antipyretic efficacy and parasite clearance effects (Malaria
545 FEVER study). *PLOS ONE* **17**, e0268414 (2022).
546 8. Suz, P., Vavilala, M. S., Souter, M., Muangman, S. & Lam, A. M. Clinical Features of Fever
547 Associated With Poor Outcome in Severe Pediatric Traumatic Brain Injury. *Journal of Neurosurgical*
548 *Anesthesiology* **18**, 5 (2006).
549 9. Greer, D. M., Funk, S. E., Reaven, N. L., Ouzounelli, M. & Uman, G. C. Impact of Fever on
550 Outcome in Patients With Stroke and Neurologic Injury. *Stroke* **39**, 3029–3035 (2008).
551 10. Birbeck, G. L. *et al.* Acetaminophen and Ibuprofen in Pediatric Central Nervous System Malaria: A
552 Randomized Clinical Trial. *JAMA Neurology* **81**, 857–865 (2024).

553 11. Miller, L. H., Baruch, D. I., Marsh, K. & Doumbo, O. K. The pathogenic basis of malaria. *Nature*
554 **415**, 673–679 (2002).
555 12. Smith, J. D. *et al.* Switches in Expression of Plasmodium falciparum var Genes Correlate with
556 Changes in Antigenic and Cytoadherent Phenotypes of Infected Erythrocytes. *Cell* **82**, 101–110
557 (1995).
558 13. Su, X. Z. *et al.* The large diverse gene family var encodes proteins involved in cytoadherence and
559 antigenic variation of Plasmodium falciparum-infected erythrocytes. *Cell* **82**, 89–100 (1995).
560 14. Sahu, P. K. *et al.* Determinants of brain swelling in pediatric and adult cerebral malaria. *JCI Insight* **6**,
561 e145823 (2021).
562 15. Jones, D. *et al.* Physiological febrile heat stress increases cytoadhesion through increased protein
563 trafficking of Plasmodium falciparum surface proteins into the red blood cell. *eLife* **14**, (2025).
564 16. Oakley, M. S. M. *et al.* Molecular Factors and Biochemical Pathways Induced by Febrile
565 Temperature in Intraerythrocytic *Plasmodium falciparum* Parasites. *Infect Immun* **75**, 2012–2025
566 (2007).
567 17. Udomsangpetch, R. *et al.* Febrile temperatures induce cytoadherence of ring-stage *Plasmodium*
568 *falciparum* -infected erythrocytes. *Proc. Natl. Acad. Sci. U.S.A.* **99**, 11825–11829 (2002).
569 18. Carvalho, P. A., Diez-Silva, M., Chen, H., Dao, M. & Suresh, S. Cytoadherence of erythrocytes
570 invaded by Plasmodium falciparum: Quantitative contact-probing of a human malaria receptor. *Acta*
571 *Biomaterialia* **9**, 6349–6359 (2013).
572 19. Zhang, R., Chandramohanadas, R., Lim, C. T. & Dao, M. Febrile Temperature Elevates the
573 Expression of Phosphatidylserine on Plasmodium falciparum (FCR3CSA) Infected Red Blood Cell
574 Surface Leading to Increased Cytoadhesion. *Sci Rep* **8**, 15022 (2018).
575 20. Marinkovic, M. *et al.* Febrile temperature leads to significant stiffening of *Plasmodium falciparum*
576 parasitized erythrocytes. *American Journal of Physiology-Cell Physiology* **296**, C59–C64 (2009).

577 21. Lubiana, P. *et al.* Adhesion between P. falciparum infected erythrocytes and human endothelial
578 receptors follows alternative binding dynamics under flow and febrile conditions. *Sci Rep* **10**, 4548
579 (2020).
580 22. Dörpinghaus, M. *et al.* Stringent Selection of Knobby Plasmodium falciparum-Infected Erythrocytes
581 during Cytoadhesion at Febrile Temperature. *Microorganisms* **8**, 174 (2020).
582 23. Tulapurkar, M. E. *et al.* Febrile-Range Hyperthermia Modifies Endothelial and Neutrophilic
583 Functions to Promote Extravasation. *Am J Respir Cell Mol Biol* **46**, 807–814 (2012).
584 24. Keitelman, I. A. *et al.* Short-Term Fever-Range Hyperthermia Accelerates NETosis and Reduces Pro-
585 inflammatory Cytokine Secretion by Human Neutrophils. *Front. Immunol.* **10**, (2019).
586 25. Koutsiaris, A. G. *et al.* Volume flow and wall shear stress quantification in the human conjunctival
587 capillaries and post-capillary venules in vivo. *Biorheology* **44**, 375–386 (2007).
588 26. Itoh, Y. & Suzuki, N. Control of brain capillary blood flow. *J Cereb Blood Flow Metab* **32**, 1167–
589 1176 (2012).
590 27. Kaul, D. K., Roth, E. J., Nagel, R. L., Howard, R. J. & Handunnetti, S. M. Rosetting of in
591 *Plasmodium falciparum*-infected red blood cells with uninfected red blood cells enhances
592 microvascular obstruction under flow conditions. *Blood* **78**, 812–819 (1991).
593 28. Sahu, P. K. *et al.* Pathogenesis of cerebral malaria: new diagnostic tools, biomarkers, and therapeutic
594 approaches. *Front Cell Infect Microbiol* **5**, 75 (2015).
595 29. Hempel, C., Wang, C. W., Kurtzhals, J. A. & Staalsø, T. Binding of *Plasmodium falciparum* to CD36
596 can be shielded by the glycocalyx. *Malar J* **16**, 193 (2017).
597 30. Targosz-Korecka, M. *et al.* Endothelial glycocalyx shields the interaction of SARS-CoV-2 spike
598 protein with ACE2 receptors. *Sci Rep* **11**, 12157 (2021).
599 31. Introini, V., Carciati, A., Tomaiuolo, G., Cicuta, P. & Guido, S. Endothelial glycocalyx regulates
600 cytoadherence in *Plasmodium falciparum* malaria. *J. R. Soc. Interface* **15**, 20180773 (2018).
601 32. Corbett, C. E., Duarte, M. I., Lancellotti, C. L., Silva, M. A. & Andrade Júnior, H. F. Cytoadherence
602 in human falciparum malaria as a cause of respiratory distress. *J Trop Med Hyg* **92**, 112–120 (1989).

603 33. Van den Steen, P. E. *et al.* Pathogenesis of malaria-associated acute respiratory distress syndrome.
604 *Trends in Parasitology* **29**, 346–358 (2013).
605 34. Bush, M. A. *et al.* Degradation of endothelial glycocalyx in Tanzanian children with Falciparum
606 malaria. *FASEB J* **35**, e21805 (2021).
607 35. Barber, B. E. *et al.* Endothelial glycocalyx degradation and disease severity in Plasmodium vivax and
608 Plasmodium knowlesi malaria. *Sci Rep* **11**, 9741 (2021).
609 36. Park, P. W., Pier, G. B., Hinkes, M. T. & Bernfield, M. Exploitation of syndecan-1 shedding by
610 Pseudomonas aeruginosa enhances virulence. *Nature* **411**, 98–102 (2001).
611 37. Mulivor, A. W. & Lipowsky, H. H. Inhibition of Glycan Shedding and Leukocyte-Endothelial
612 Adhesion in Postcapillary Venules by Suppression of Matrixmetalloprotease Activity with
613 Doxycycline. *Microcirculation* **16**, 657–666 (2009).
614 38. Bernabeu, M. *et al.* Severe adult malaria is associated with specific PfEMP1 adhesion types and high
615 parasite biomass. *Proc Natl Acad Sci U S A* **113**, E3270-3279 (2016).
616 39. Kessler, A. *et al.* Linking EPCR-Binding PfEMP1 to Brain Swelling in Pediatric Cerebral Malaria.
617 *Cell Host Microbe* **22**, 601-614.e5 (2017).
618 40. Gillrie, M. R. *et al.* Src-family kinase–dependent disruption of endothelial barrier function by
619 Plasmodium falciparum merozoite proteins. *Blood* **110**, 3426–3435 (2007).
620 41. Gallego-Delgado, J. *et al.* Angiotensin receptors and β-catenin regulate brain endothelial integrity in
621 malaria. *J Clin Invest* **126**, 4016–4029 (2016).
622 42. Howard, C., Joof, F., Hu, R., Smith, J. D. & Zheng, Y. Probing cerebral malaria inflammation in 3D
623 human brain microvessels. *Cell Rep* **42**, 113253 (2023).
624 43. Piatti, L. *et al.* Plasmodium falciparum egress disrupts endothelial junctions and activates JAK-STAT
625 signaling in a microvascular 3D blood-brain barrier model. *Nat Commun* **16**, 7262 (2025).
626 44. Knackstedt, S. L. *et al.* Neutrophil extracellular traps drive inflammatory pathogenesis in malaria. *Sci*
627 *Immunol* **4**, eaaw0336 (2019).

628 45. Du, X. *et al.* PRL2 regulates neutrophil extracellular trap formation which contributes to severe
629 malaria and acute lung injury. *Nat Commun* **15**, 881 (2024).
630 46. Yang, S.-C., Tsai, Y.-F., Pan, Y.-L. & Hwang, T.-L. Understanding the role of neutrophils in acute
631 respiratory distress syndrome. *Biomed J* **44**, 439–446 (2021).
632 47. Birbeck, G. L. *et al.* Blantyre Malaria Project Epilepsy Study (BMPES) of neurological outcomes in
633 retinopathy-positive paediatric cerebral malaria survivors: a prospective cohort study. *The Lancet*
634 *Neurology* **9**, 1173–1181 (2010).
635 48. Yeo, T. W. *et al.* Glycocalyx breakdown is associated with severe disease and fatal outcome in
636 *Plasmodium falciparum* malaria. *Clin Infect Dis* **69**, 1712–1720 (2019).
637 49. Yeo, T. W. *et al.* Glycocalyx breakdown is increased in African children with cerebral and
638 uncomplicated falciparum malaria. *The FASEB Journal* **33**, 14185–14193 (2019).
639 50. Georgiadou, A. & Cunnington, A. J. Shedding of the vascular endothelial glycocalyx: a common
640 pathway to severe malaria? *Clin Infect Dis* **69**, 1721–1723 (2019).
641 51. Lyimo, E. *et al.* In Vivo Imaging of the Buccal Mucosa Shows Loss of the Endothelial Glycocalyx
642 and Perivascular Hemorrhages in Pediatric Plasmodium falciparum Malaria. *Infect Immun* **88**,
643 e00679-19 (2020).
644 52. Giantsos-Adams, K. M. *et al.* Heparan Sulfate Regrowth Profiles Under Laminar Shear Flow
645 Following Enzymatic Degradation. *Cell Mol Bioeng* **6**, 160–174 (2013).
646 53. Potter, D. R., Jiang, J. & Damiano, E. R. The recovery time course of the endothelial-cell glycocalyx
647 in vivo and its implications in vitro. *Circ Res* **104**, 1318–1325 (2009).
648 54. Reitsma, S., Slaaf, D. W., Vink, H., van Zandvoort, M. A. M. J. & oude Egbrink, M. G. A. The
649 endothelial glycocalyx: composition, functions, and visualization. *Pflugers Arch* **454**, 345–359
650 (2007).
651 55. Schmidt, E. P. *et al.* The pulmonary endothelial glycocalyx regulates neutrophil adhesion and lung
652 injury during experimental sepsis. *Nat Med* **18**, 1217–1223 (2012).

653 56. Ando, Y. *et al.* Brain-Specific Ultrastructure of Capillary Endothelial Glycocalyx and Its Possible
654 Contribution for Blood Brain Barrier. *Sci Rep* **8**, 17523 (2018).
655 57. Kirchhausen, T., Staunton, D. E. & Springert, T. A. Location of the domains of ICAM-1 by
656 immunolabeling and single-molecule electron microscopy. *Journal of Leukocyte Biology* **53**, 342–346
657 (1993).
658 58. Jun, C.-D. *et al.* Ultrastructure and Function of Dimeric, Soluble Intercellular Adhesion Molecule-1
659 (ICAM-1)*. *Journal of Biological Chemistry* **276**, 29019–29027 (2001).
660 59. Lukasz, A. *et al.* Endothelial glycocalyx breakdown is mediated by angiopoietin-2. *Cardiovascular*
661 *Research* **113**, 671–680 (2017).
662 60. Deininger, M. H., Winkler, S., Kremsner, P. G., Meyermann, R. & Schluesener, H. J. Angiogenic
663 proteins in brains of patients who died with cerebral malaria. *Journal of Neuroimmunology* **142**, 101–
664 111 (2003).
665 61. Jain, V. *et al.* Plasma levels of angiopoietin-1 and -2 predict cerebral malaria outcome in Central
666 India. *Malaria Journal* **10**, 383 (2011).
667 62. Conroy, A. L. *et al.* Angiopoietin-2 levels are associated with retinopathy and predict mortality in
668 Malawian children with cerebral malaria: A retrospective case–control study*. *Critical Care*
669 *Medicine* **40**, 952 (2012).
670 63. Taraboletti, G. *et al.* Shedding of the Matrix Metalloproteinases MMP-2, MMP-9, and MT1-MMP as
671 Membrane Vesicle-Associated Components by Endothelial Cells. *The American Journal of Pathology*
672 **160**, 673–680 (2002).
673 64. Endo, K. *et al.* Cleavage of syndecan-1 by membrane type matrix metalloproteinase-1 stimulates cell
674 migration. *J Biol Chem* **278**, 40764–40770 (2003).
675 65. Allweier, J. *et al.* Cytoadhesion of Plasmodium falciparum-Infected Red Blood Cells Changes the
676 Expression of Cytokine-, Histone- and Antiviral Protein-Encoding Genes in Brain Endothelial Cells.
677 *Mol Microbiol* **122**, 948–967 (2024).

678 66. Fitzgerald, M., Hayward, I. P., Thomas, A. C., Campbell, G. R. & Campbell, J. H. Matrix
679 metalloproteinase can facilitate the heparanase-induced promotion of phenotype change in vascular
680 smooth muscle cells. *Atherosclerosis* **145**, 97–106 (1999).
681 67. Ramnath, R. D. *et al.* Blocking matrix metalloproteinase-mediated syndecan-4 shedding restores the
682 endothelial glycocalyx and glomerular filtration barrier function in early diabetic kidney disease.
683 *Kidney Int* **97**, 951–965 (2020).
684 68. Hempel, C., Sporring, J. & Kurtzhals, J. A. L. Experimental cerebral malaria is associated with
685 profound loss of both glycan and protein components of the endothelial glycocalyx. *The FASEB*
686 *Journal* **33**, 2058–2071 (2019).
687 69. Dove, A. MMP inhibitors: Glimmers of hope amidst clinical failures. *Nature Medicine* **8**, 95–95
688 (2002).
689 70. Khachaturyan, G. *et al.* Temperature-sensitive migration dynamics in neutrophil-differentiated HL-60
690 cells. *Sci Rep* **12**, 7053 (2022).
691 71. Janko, J. *et al.* Neutrophil extracellular traps formation and clearance is enhanced in fever and
692 attenuated in hypothermia. *Front. Immunol.* **14**, (2023).
693 72. Lefor, A. T. *et al.* Hyperthermia increases intercellular adhesion molecule-1 expression and
694 lymphocyte adhesion to endothelial cells. *Surgery* **116**, 214–220; discussion 220-221 (1994).
695 73. Chen, Q. *et al.* Thermal Facilitation of Lymphocyte Trafficking Involves Temporal Induction of
696 Intravascular ICAM-1. *Microcirculation* **16**, 143–158 (2009).
697 74. Chen, Q. *et al.* Fever-range thermal stress promotes lymphocyte trafficking across high endothelial
698 venules via an interleukin 6 trans-signaling mechanism. *Nat Immunol* **7**, 1299–1308 (2006).
699 75. Shah, A. *et al.* Cytokine and adhesion molecule expression in primary human endothelial cells
700 stimulated with fever-range hyperthermia. *Int J Hyperthermia* **18**, 534–551 (2002).
701 76. Yazdan-Ashoori, P. *et al.* Elevated plasma matrix metalloproteinases and their tissue inhibitors in
702 patients with severe sepsis. *J Crit Care* **26**, 556–565 (2011).

703 77. Alam, M., Mohammad, A., Rahman, S., Todd, K. & Shuaib, A. Hyperthermia up-regulates matrix
704 metalloproteinases and accelerates basement membrane degradation in experimental stroke.
705 *Neuroscience Letters* **495**, 135–139 (2011).
706 78. Taghavi, S. *et al.* Glycocalyx degradation and the endotheliopathy of viral infection. *PLOS ONE* **17**,
707 e0276232 (2022).
708 79. Shi, S. M. *et al.* Glycocalyx dysregulation impairs blood–brain barrier in ageing and disease. *Nature*
709 **639**, 985–994 (2025).
710 80. Laptook, A. R. & Corbett, R. J. T. The effects of temperature on hypoxic-ischemic brain injury.
711 *Clinics in Perinatology* **29**, 623–649 (2002).
712 81. Kiyatkin, E. A. & Sharma, H. S. Permeability of the blood–brain barrier depends on brain
713 temperature. *Neuroscience* **161**, 926–939 (2009).
714 82. Lim, Y. B. *et al.* Temperature-Induced Catch-Slip to Slip Bond Transit in *Plasmodium falciparum*-
715 Infected Erythrocytes. *Biophysical Journal* **118**, 105–116 (2020).
716 83. Bernabeu, M. *et al.* Binding Heterogeneity of Plasmodium falciparum to Engineered 3D Brain
717 Microvessels Is Mediated by EPCR and ICAM-1. *mBio* **10**, e00420-19 (2019).
718 84. Joof, F. *et al.* Plasma From Older Children in Malawi Inhibits Plasmodium falciparum Binding in 3-
719 Dimensional Brain Microvessels. *J Infect Dis* **230**, e1402–e1411 (2024).
720 85. Reyes, R. A. *et al.* Broadly inhibitory antibodies to severe malaria virulence proteins. *Nature* **636**,
721 182–189 (2024).
722 86. Lipowsky, H. H. Microvascular Rheology and Hemodynamics. *Microcirculation* **12**, 5–15 (2005).
723 87. Hughes, C. S. *et al.* Ultrasensitive proteome analysis using paramagnetic bead technology. *Molecular*
724 *Systems Biology* **10**, 757 (2014).
725 88. Hughes, C. S. *et al.* Single-pot, solid-phase-enhanced sample preparation for proteomics experiments.
726 *Nat Protoc* **14**, 68–85 (2019).
727 89. Dayon, L. *et al.* Relative Quantification of Proteins in Human Cerebrospinal Fluids by MS/MS Using
728 6-Plex Isobaric Tags. *Anal. Chem.* **80**, 2921–2931 (2008).

90. Kong, A. T., Leprevost, F. V., Avtonomov, D. M., Mellacheruvu, D. & Nesvizhskii, A. I. MSFragger: ultrafast and comprehensive peptide identification in mass spectrometry–based proteomics. *Nat Methods* **14**, 513–520 (2017).

91. Ritchie, M. E. *et al.* limma powers differential expression analyses for RNA-sequencing and microarray studies. *Nucleic Acids Research* **43**, e47 (2015).

92. Huber, W., von Heydebreck, A., Sültmann, H., Poustka, A. & Vingron, M. Variance stabilization applied to microarray data calibration and to the quantification of differential expression. *Bioinformatics* **18 Suppl 1**, S96-104 (2002).